Research Square

Preprints are preliminary reports that have not undergone peer review.
They should not be considered conclusive, used to inform clinical practice,
or referenced by the media as validated information.

Synergistic Effects of Solution Treatment, Aging, and Shot Peening on the Microstructure, Mechanical Properties, and Surface Integrity of SLM-Fabricated AlSi10Mg Alloy

Kadir AYDIN

kadir.aydin@dpu.edu.tr

Kütahya Dumlupınar Üniversitesi

Research Article

Keywords: Additive Manufacturing, Aging, Shot peening, AlSi10Mg, Post-processing

Posted Date: November 6th, 2026

DOI: https://doi.org/10.21203/rs.3.rs-11430490/v1

License: This work is licensed under a Creative Commons Attribution 4.0 International License.
Read Full License

Additional Declarations: No competing interests reported.

Abstract

This study investigates the effects of shot peening (SP) performed after solution treatment (ST) and aging on the microstructure, mechanical properties, and surface quality of AlSi10Mg alloy produced by selective laser melting (SLM). ST was conducted at 540°C for 2 hours, followed by aging at 180°C for 6 hours, whereas SP was performed using various processing parameters. Microstructural examinations, tensile tests, and analyses of microhardness, density, and 3D surface topography were performed. The results indicated that ST and aging reduced tensile strength while increasing elongation at break. SP increased the yield strength of the heat-treated samples; for the sample subjected to SP after aging, this value exceeded that of the as-built condition (reaching 267 MPa). Furthermore, SP reduced surface roughness across all processing conditions. The lowest Ra and Rq values, 0.30 μm and 0.40 μm, respectively, were observed in the sample subjected to SP after ST. Conversely, the near-surface microcracks and reduced ductility observed after SP highlighted the need for a comprehensive evaluation of mechanical properties. The findings demonstrate that SP is a complementary process that enhances the mechanical properties and surface quality of the heat-treated AlSi10Mg; however, processing parameters must be optimized with due consideration for surface integrity and ductility.

1. Introduction

Aluminum alloys are widely used in the automotive and aerospace sectors, where high strength and light weight are preferred. AlSi10Mg is an aluminum alloy classified among Al-Si-based hypoeutectic alloys. Preferred for applications requiring high corrosion resistance, a narrow solidification range, low weight, and high strength, the AlSi10Mg alloy can be produced via both casting and SLM methods [1–4].

SLM is based on the principle of manufacturing parts directly using computer-aided design (CAD) data. SLM enables the production of complex parts that cannot be manufactured using traditional methods. This innovative technology allows for the production of denser parts through layer-by-layer manufacturing. Furthermore, compared to conventional methods, it stands out for its advantages, including efficiency, minimal material waste, shorter production times, and design flexibility. However, additive manufacturing also presents certain disadvantages. Complex thermal cycles occurring during production, particularly in laser powder bed technology, are a notable factor. These thermal cycles lead to undesirable phenomena such as stress accumulation, residual stresses, porosity, and surface roughness [5, 6]. Post-processing operations are employed to eliminate these issues. Heat treatment is used to alleviate residual stresses and stress accumulations induced by thermal cycles. Solution treatment (ST) and aging are among these heat treatments. An elongation at break of up to 20% has been observed following ST, indicating a significant reduction in residual stresses [7]. Additionally, a decrease in the low-angle grain boundary (LAGB) fraction observed by EBSD after T6 heat treatment signals a reduction in internal stresses [8]. However, it has been reported that after ST and aging, the ultra-fine eutectic microstructure is replaced by precipitated Si particles, leading to a dramatic drop in strength [9]. It has been determined that both yield and tensile strengths decrease in solution-treated samples, and that the alloy's strength diminishes as the solution-treatment temperature rises [10]. ST

also reduces hardness values. Furthermore, it has been reported that increasing the solution-treatment temperature increases the size of Si particles [11]. A review of the literature clearly indicates that solution treatment and aging processes eliminate material brittleness by reducing residual stresses. However, it has been observed that the ultra-fine eutectic structure characteristic of additive manufacturing degrades, resulting in significant reductions in strength and hardness. SP is applied to create a plastic deformation layer near the surface, serving purposes such as grain refinement, crack prevention, the induction of compressive residual stress, increased hardness, and porosity reduction [12–14]. Additionally, it has been reported that the SP process eliminates surface defects and enhances the mechanical properties of AlSi10Mg [15]. The formation of nanostructured grains on the surface following SP is also a factor contributing to increased hardness. Moreover, it has been reported that SP creates subsurface plastic deformation layers, thereby shifting the site of crack initiation away from the surface [16]. It has also been noted that SP improves fatigue strength by reducing porosity at and near the surface [17].

In AlSi10Mg alloys produced via the SLM method, ST and aging heat treatments are frequently employed in the literature to eliminate microstructural defects and enhance ductility. However, these processes disrupt the ultrafine eutectic structure, a hallmark of additive manufacturing, leading to a dramatic decline in the material's strength and hardness. Conversely, shot peening, a mechanical surface treatment, is known to reduce surface roughness and improve fatigue life by inducing residual compressive stresses. Despite this, the sequential and synergistic effects of these two post-processing mechanisms- specifically, how the loss of strength caused by heat treatment might be compensated for through shot peening parameters, and the resulting structural alterations to surface integrity (such as the formation of micro-cracks) have yet to be systematically mapped in the literature. This study aims to bridge this gap by systematically investigating the combined effects of solution treatment and aging, followed by shot peening, on the microstructure, mechanical properties, and 3D surface integrity of SLM-produced AlSi10Mg alloys. By evaluating the increased ductility from heat treatment alongside the surface hardening and smoothing effects of shot peening, an optimal sequential post-processing strategy for additively manufactured components is established.

2. Material and Method

2.1. The AM-SLM and post-processing

The AlSi10Mg material used in the study was produced on an ENAVISION250 machine using the SLM technique. Production was carried out with the following parameters: laser power of 240 W, scanning speed of 1300 mm/s, hatch spacing of 0.1 mm, and layer thickness of 30 µm. Additionally, argon was used as the shielding gas during production. Solution treatment and aging were applied to the additively manufactured AlSi10Mg specimens; the heat-treatment heating rate was 20°C/min. Following the heat treatment, the specimens underwent SP. The SP process was performed using ASH 230 steel shot. The process parameters were as follows: projection pressure of 3.5 bar, peening duration of 10 s, surface

coverage of 200%, nozzle angle of 90 degrees, and nozzle distance of 500 mm. Details of the applied processes are presented in Table 1.

Table 1
Details of the different processes applied

Number of specimens	Process	Procedure
S1	As-Built	SLMed AlSi10Mg
S2	ST	540 ℃/2 h/Water quench (WQ)
S3	Aging	540 ℃/2 h/WQ + 180 ℃/ 6 h/Air cool (AC)
S4	SP	SP
S5	ST + SP	540 ℃/2 h/ WQ + SP
S6	Aging + SP	540 ℃/2 h/ WQ + 180 ℃/ 6 h/ AC + SP

2.2. Testing and analysis of samples

Metallographic examination, hardness testing, and tensile testing were performed on the samples subjected to SP after aging. During the metallographic preparation stage, the samples were ground up to 2500 mesh. After being polished with a diamond solution, the samples were etched using Keller's reagent for 20 seconds. Preparations for imaging via optical microscopy and scanning electron microscopy (SEM) were completed. Tensile test specimens, prepared in accordance with the ASTM E8 standard, were subjected to tensile testing at room temperature and a speed of 1 mm/min using a Zwick/Roell Z-100 tensile testing machine. Microhardness testing was conducted using a Duroline-M microhardness tester with a 200 g load for 10 seconds. Surface topography analysis was performed using a 3D optical profilometer. These analyses were carried out in accordance with the ISO 4287 standard regarding arithmetic mean (Ra) and root-mean-square (Rq) parameters. A schematic representation of the processes performed is provided in Fig. 1.

3. Results and discussion

3.1. The evaluation of microstructure

Figure 2 presents images related to the post-processing of the AlSi10Mg alloy produced via additive manufacturing. Figure 2a shows an optical microscope image of the AlSi10Mg sample in the as-built state. The image reveals the characteristic microstructural features formed by melt pools and laser scanning paths specific to the SLM process; a fish-scale pattern of molten pools and molten boundaries is visible in the optical microscope image. The average height (h) and width (w) of the melt pools were approximately 91.6 µm and 171.4 µm, respectively. The melt pool aspect ratio (h/w) is 0.53. This is quite close to the conventionally assumed value of 0.5 [18]. Figure 2b shows the SEM image of the shot-peened sample. Significant surface deformation occurred during SP, altering the surface morphology

compared to the as-built condition. Micro-cracks in the near-surface regions are also notable. Indeed, it has been reported that excessive plastic deformation of the parts, particularly in cases of over-peening and perpendicular-angle peening, leads to the formation of near-surface micro-cracks [19, 20]. Figure 2c displays an SEM image of the as-built AlSi10Mg sample along with an EDX analysis of a selected region. The SEM image shows a fine distribution of fibrous Si networks within the α-Al matrix. Furthermore, since no precipitation occurred in the as-built part, the Si phases are eutectic, and the dendritic structure of the as-built sample is visible. α-Al cell dimensions and eutectic Si network morphology profoundly influence the strengthening mechanisms of the SLM AlSi10Mg alloy [21]. The EDX spectrum indicates the presence of Al, Si, and Mg as the primary elements. The EDX analysis yielded an elemental distribution of approximately 87.4% Al, 12.0% Si, and 0.6% Mg. These results demonstrate that the material has a chemical composition consistent with that of the AlSi10Mg alloy. Figure 2d presents the SEM image, EDX spectrum, and elemental maps for sample S2. In the SEM image, Si-rich regions exhibiting distinct contrast within the Al matrix are clearly observable. Following the ST treatment, the dendritic structure gave way to precipitated Si particles [8]. Localized EDX analysis of the precipitated grains reveals that the precipitated particles are highly rich in Si. Si content of 43.2% was detected in the point EDX analysis performed on the precipitated grain shown in Fig. 2d. Figure 2e presents the SEM image, EDX spectrum, and elemental maps for sample S3. During aging, fine Mg_2Si precipitates form within the aluminum matrix via precipitation hardening. Although these nanoprecipitates, smaller than 100 nm, are not directly visible, they play an effective role in strengthening the material. By inhibiting dislocation motion through the Orowan mechanism, these precipitates increase the material's resistance to plastic flow [22–25].

3.2. Mechanical properties

The tensile test results of the examined samples are presented in Table 2 and Fig. 3a. It was observed that the tensile test results varied significantly with the applied heat treatment and SP processes, and that, compared with the as-built condition, ST and aged samples exhibited decreased tensile strength and increased elongation at break. In the S2 sample, a substantial reduction was observed in both yield and tensile strengths (100 MPa and 221 MPa, respectively), while a significant increase in elongation at break (12.5%) was noted. The effect of grain size on mechanical properties can be explained by the Hall-Petch relationship [11]. The Hall-Petch relation is shown in Eq. 1. In the equation, σ is the yield strength, σ_0 and k are material constants, and d is the grain size.

$$\sigma = \sigma_0 + k.d^{-1/2} \quad (1)$$

Grain refinement reduces the inter-particle spacing of Si, thereby enhancing strength, as the increased Al-Si interfacial area impedes dislocation movement [23, 26]. This explains why the highest tensile strength (400 MPa) was exhibited by the ultra-fine-grained as-built sample. The structure and size of the Si phases formed after heat treatment directly influence strength and ductility [27]. Following ST and aging, Si particles precipitating from the supersaturated Al matrix reduce strength by decreasing the number of Si grains and increasing grain size [28]. Residual stresses decrease after the ST process,

thereby increasing ductility; however, elongation at break decreases slightly after aging (S3; 6%). The yield strength results obtained from the tensile tests on SP specimens (S4, S5, and S6) are noteworthy. Increases in yield strength were observed as follows: approximately 7% from S1 to S4, 38% from S2 to S5, and 15% from S3 to S6. The increase is particularly striking following the heat treatment. Compressive residual stresses induced by the SP process play a critical role in enhancing yield strength [29]. Conversely, the significant reduction in ductility observed in the SP specimens is attributed to cracking in the near-surface regions caused by plastic deformation during the SP process. Indeed, Jamalian et al. have reported a similar phenomenon [30].

Table 2
Tensile test values of the samples

Specimens	YS (MPa)	UTS (MPa)	EL (%)
S1	236 ± 1	400 ± 3	3.8 ± 0.2
S2	110 ± 2	221 ± 4	12.5 ± 1.5
S3	232 ± 10	278 ± 11	6 ± 0.7
S4	252 ± 9	364 ± 2	2 ± 0.1
S5	152 ± 9	236 ± 4	5.7 ± 0.1
S6	267 ± 2	293 ± 1	3.1 ± 0.3

The microhardness results for the experimental samples are presented in Fig. 3b. The average hardness of the as-built sample (S1) was 125.4 HV. The higher hardness value in the as-built sample is attributed to the dislocation structure, the fine distribution of eutectic Si within the Al matrix, and the cellular dendritic microstructure [7]. For sample S2, which underwent ST, the hardness value dropped to 70 HV. This reduction in hardness in sample S2 can be associated with the dissolution of existing hardening phases and the material's transition to a softer microstructure during the ST process [31]. The hardness of sample S3 was measured at 98 HV, indicating a slight increase relative to sample S2. It has been reported that the precipitation of the Mg_2Si phase or other metastable phases leads to a limited increase in hardness values [7]. The average hardness values reached 107.3 HV for sample S4, 103.2 HV for sample S5, and 110.5 HV for sample S6. These results indicate that the plastic deformation and work hardening induced by the SP process, particularly in the surface region, significantly influence the hardness values [15].

Archimedes' density tests were performed on the experimental samples, and the results are presented in Fig. 3c. The relative density of the as-built sample was determined to be 2.63 g/cm³ (98.4%). However, a slight decrease in density was observed in the ST and aged samples. This is attributed to the dissolution of eutectic Si fibers, which disrupts the cellular structure and facilitates the coalescence of internal pores [32–34]. Furthermore, the reduction in density was slightly more pronounced in the aged samples due to the longer heat-treatment duration. An increase in density values was observed in all samples

following the SP process. In terms of relative density, there is an increase of approximately 1% from S1 to S4, approximately 1.5% from S2 to S5, and approximately 2.3% from S3 to S6. SP increased the relative density; this effect can be attributed to the closure or shrinkage of near-surface pores due to deformation [17].

3.3. Surface Morphology and Roughness Analyses

Figure 4 presents the three-dimensional surface topographies and the Ra and Rq surface roughness values for samples S1–S6. When the sample groups are evaluated collectively, it is evident that the applied ST, aging, and SP processes resulted in distinct differences in surface topography. The Ra and Rq values for the as-built sample (S1) were measured as 0.63 µm and 0.95 µm, respectively. No significant change in surface roughness was observed in the ST sample (S2) or the aged sample (S3). Literature also notes that the effect of heat treatment on surface roughness is quite limited [35].

The most notable change is observed in the shot-peened samples. For sample S4, Ra and Rq values were determined to be 0.34 µm and 0.48 µm, respectively. Compared to the as-built sample S1, Ra decreased by approximately 45.3% and Rq by approximately 49.4%. Similarly, Subramaniyan et al. reported that the post-process SP treatment reduced the surface roughness of as-built parts by approximately 50% [36]. This is attributed to the effective removal of surface defects that characterize SLM parts (satellite particles, agglomerates, partially melted particles, and open porosity). For sample S5 subjected to ST followed by SP, Ra was measured at 0.30 µm and Rq at 0.40 µm. Comparing S5 with its counterpart, sample S2, reveals a reduction of approximately 48.3% in Ra and 66.7% in Rq. For sample S6, subjected to aging followed by SP, the Ra and Rq values were 0.34 µm and 0.48 µm, respectively; compared with the aged sample S3, both Ra and Rq decreased by approximately 54.8%. These results demonstrate that the SP process significantly reduces surface roughness on surfaces prepared under various heat-treatment conditions. Notably, sample S5 exhibits the lowest Ra (0.30 µm) and Rq (0.40 µm) values among all samples, indicating that the combination of ST and SP yields the lowest measured surface roughness under the investigated processing conditions. Three-dimensional surface imagery supports this finding, showing that the S5 surface displays a more homogeneous topographic distribution.

4. Conclusions

In this study, the effects of heat treatment and shot peening processes on the microstructural, mechanical, and surface properties of SLM-produced AlSi10Mg alloy were investigated. The results obtained are summarized below.

1) The cellular eutectic Si network and melt pool boundaries observed in the as-built (S1) condition completely dissolved and transformed into coarse Si particles within the matrix following the ST (S2) at 540°C. These microstructural changes are associated with differences in the mechanical behavior of the samples. Additionally, microcracks were detected in the near-surface regions after SP, depending on the peening parameters.

2) ST and aging processes reduced tensile strength while increasing elongation at break. SP significantly increased yield strength, particularly in heat-treated samples. However, a loss of ductility and the presence of near-surface microcracks were observed in the shot-peened samples.

3) Microhardness, which was 125.4 HV in the as-built sample, dropped to 70 HV after ST. In shot-peened samples, microhardness values were measured in the range of 103.2–110.5 HV. Furthermore, an increase in relative density was observed after SP; this may be attributed to the shrinkage or closure of near-surface pores due to deformation.

4) SP reduced surface roughness under all processing conditions investigated. The lowest Ra (0.30 μm) and Rq (0.40 μm) values were obtained for the sample subjected to ST followed by SP. This result demonstrates that SP can improve surface quality under appropriate processing conditions.

5) Overall, it is concluded that the SP process partially compensates for the loss of strength and hardness resulting from heat treatment and improves surface quality and density, albeit at the cost of reduced ductility. In this context, the combination of ST and SP (S5) is considered a promising post-processing strategy for applications requiring both high strength and superior surface quality. Future studies should focus on minimizing ductility loss by optimizing SP parameters (shot size, blasting pressure, duration) and conducting a detailed investigation of fatigue behavior.

Declarations

Conflict of interest: The authors declare no conflicts of interest.

Data availability: Data published in this manuscript are available for readers upon request.

Funding: This work has been supported by Kütahya Dumlupınar University Scientific Research Projects Coordination Office under grant number #2025-42.

Author Contribution Statement: The author confirms being the sole contributor of this work and has approved it for publication.

References

1. Palanisamy, C., Raman, R., Mondal, C., Dhanaraj, P., Shanmugam, S.: The synergistic effects of heat treatment and anodizing on the blackening phenomenon of DMLS-built AlSi10Mg components for aerospace applications. Proceedings of the Institution of Mechanical Engineers, Part E: Journal of Process Mechanical Engineering, 09544089251401675. (2025)
2. Duan, W., Guan, Y., Xie, Y., Huang, Y., Huang, K., Ni, X.: Influence of High-Power Laser Powder Bed Fusion Process on the Densification Behavior of AlSi10Mg Alloy. Lasers Manuf. Mater. Process., 1–18. (2026)

3. Khan, H.M., O¨ zer, G., Yilmaz, M.S., Koc¸, E.: Corrosion of Additively Manufactured Metallic Components: A Review, Arab. J. Sci. Eng. **47**(5), 5465–5490 (2022)
4. Cui, L., Wu, D., Ma, L., Qiao, J., Wu, X., He, D.: Effect of Al–Mg filler wires on weldability of cold metal transfer welded AlSi10Mg alloys fabricated using laser powder bed fusion. Metall. Mater. Trans. A. **56**(3), 840–864 (2025)
5. Liu, S., Shin, Y.C.: Additive manufacturing of Ti6Al4V alloy: A review. Mater. Des. **164**, 107552 (2019)
6. Sadeghi, M.S., Mohseni, M., Etefagh, A.H., Khajehzadeh, M.: The effect of process parameters and scanning strategies on surface roughness of stainless steel 316L SLM parts. Proceedings of the Institution of Mechanical Engineers, Part E: Journal of Process Mechanical Engineering, 237(6), 2510–2519. (2023)
7. Majeed, A., Muzamil, M., Khan, M.A., Malik, E.H., Huzaifa, M., Lv, J., Dar, N.U.: Comprehensive Mechanical Behavior of Thin-Walled Additively-Manufactured Parts of AlSi10Mg by SLM in As-Built, Post-Solution, and Aging Treatment Conditions: Majeed, Muzamil, Khan, Malik, Huzaifa, Lv, and Dar. Jom. **75**(8), 3067–3082 (2023)
8. Tang, H., Gao, C., Zhang, Y., Zhang, N., Lei, C., Bi, Y., Rao, J.H.: Effects of direct aging treatment on microstructure, mechanical properties and residual stress of selective laser melted AlSi10Mg alloy. J. Mater. Sci. Technol. **139**, 198–209 (2023)
9. Baek, M.S., Kreethi, R., Park, T.H., Sohn, Y., Lee, K.A.: Influence of heat treatment on the high-cycle fatigue properties and fatigue damage mechanism of selective laser melted AlSi10Mg alloy. Mater. Sci. Engineering: A. **819**, 141486 (2021)
10. Zhang, H., Wang, Y., Wang, J.J., Ni, D.R., Wang, D., Xiao, B.L., Ma, Z.Y.: Achieving superior mechanical properties of selective laser melted AlSi10Mg via direct aging treatment. J. Mater. Sci. Technol. **108**, 226–235 (2022)
11. Li, W., Li, S., Liu, J., Zhang, A., Zhou, Y., Wei, Q., Shi, Y.: Effect of heat treatment on AlSi10Mg alloy fabricated by selective laser melting: Microstructure evolution, mechanical properties and fracture mechanism. Mater. Sci. Engineering: A. **663**, 116–125 (2016)
12. Liu, Y.G., Li, H.M., Li, M.Q.: Characterization of surface layer in TC17 alloy treated by air blast shot peening. Mater. Design. **65**, 120–126 (2015)
13. Unal, O., Varol, R.: Almen intensity effect on microstructure and mechanical properties of low carbon steel subjected to severe shot peening. Appl. Surf. Sci. **290**, 40–47 (2014)
14. Ahmed, A.A., Mhaede, M., Wollmann, M., Wagner, L.: Effect of micro shot peening on the mechanical properties and corrosion behavior of two microstructure Ti-6Al-4V alloy. Appl. Surf. Sci. **363**, 50–58 (2016)
15. Maamoun, A.H., Elbestawi, M.A., Veldhuis, S.C.: Influence of shot peening on AlSi10Mg parts fabricated by additive manufacturing. J. Manuf. Mater. Process. **2**(3), 40 (2018)
16. Maleki, E., Bagherifard, S., Astaraee, A.H., Sgarbazzini, S., Bandini, M., Guagliano, M.: Application of gradient severe shot peening as a novel mechanical surface treatment on fatigue behavior of additively manufactured AlSi10Mg. Mater. Sci. Engineering: A. **881**, 145397 (2023)

17. Damon, J., Dietrich, S., Vollert, F., Gibmeier, J., Schulze, V.: Process dependent porosity and the influence of shot peening on porosity morphology regarding selective laser melted AlSi10Mg parts. Additive Manuf. **20**, 77–89 (2018)
18. Patel, S., et al.: The influence of beam focus during laser powder bed fusion of a high reflectivity aluminium alloy—AlSi10Mg. Additive Manuf. **59**, 103112 (2022)
19. Maleki, E., Unal, O., Amanov, A.: Novel experimental methods for the determination of the boundaries between conventional, severe and over shot peening processes. Surf. Interfaces. **13**, 233–254 (2018)
20. Mousa, H., Omari, M.A.: Investigating the effect of shot peening parameters on the peened surface damage using FEA. Results Eng. **19**, 101355 (2023)
21. Takata, N., Liu, M., Kodaira, H., Suzuki, A., Kobashi, M.: Anomalous strengthening by supersaturated solid solutions of selectively laser melted Al–Si-based alloys. Additive Manuf. **33**, 101152 (2020)
22. Zhu, L., et al.: Achieving balanced mechanical properties in Al-Mg-Si-Cu-Zn alloys via Mg content driven multilevel ordered precipitation. J. Mater. Res. Technol., (2025)
23. Wu, L., Zhao, Z., Bai, P., Zhang, Z., Li, Y., Liang, M., Du, W.: The effect of silicon phase morphology on microstructure and properties of AlSi10Mg alloys fabricated by selective laser melting. Materials. **15**(24), 8786 (2022)
24. Chen, Y., et al.: Effect of the solid solution and aging treatment on the mechanical properties and microstructure of a novel Al-Mg-Si alloy. Materials. **16**(21), 7036 (2023)
25. Lin, Y., Zhang, J.-L., Chen, M.-S.: Evolution of precipitates during two-stage stress-aging of an Al Zn-Mg-Cu alloy. J. Alloys Compd. **684**, 177–187 (2016)
26. Semetse, L., Makin, H., Kibambe, N.M., Maja, M.E., Olubambi, P.A.: Microstructural evolution and hardness response of selective laser melted AlSi10Mg alloys during solution treatment and aging. Manuf. Lett. **49**, 929–936 (2026)
27. Chen, Y., Weyland, M., Hutchinson, C.R.: The effect of interrupted aging on the yield strength and uniform elongation of precipitation-hardened Al alloys. Acta Mater. **61**(15), 5877–5894 (2013)
28. Li, X.P., Wang, X.J., Saunders, M., Suvorova, A., Zhang, L.C., Liu, Y.J., Sercombe, T.B.: A selective laser melting and solution heat treatment refined Al–12Si alloy with a controllable ultrafine eutectic microstructure and 25% tensile ductility. Acta Mater. **95**, 74–82 (2015)
29. Karaveli, K.K., Bal, B.: Effects of strain rate and post processing on mechanical properties of additively manufactured AlSi10Mg alloys. Mater. Test. **68**(3), 479–489 (2026)
30. Jamalian, M., Field, D.P.: Effects of shot peening parameters on gradient microstructure and mechanical properties of TRC AZ31. Mater. Charact. **148**, 9–16 (2019)
31. Sathishkumar, A., Soundararajan, R., Sivasankaran, S.: Effect of direct aging on the microstructure and mechanical behavior of AlSi10Mg alloy: casting versus selective laser melting. J. Mater. Eng. Perform. **32**(7), 3215–3229 (2023)

32. Tabatabaei, N., Zarei-Hanzaki, A., Moshiri, A., Abedi, H.R.: The effect of heat treatment on the room and high temperature mechanical properties of AlSi10Mg alloy fabricated by selective laser melting. J. Mater. Res. Technol. **23**, 6039–6053 (2023)
33. Majeed, A., Muzamil, M., Lv, J., Liu, B., Ahmad, F.: Heat treatment influences densification and porosity of AlSi10Mg alloy thin-walled parts manufactured by selective laser melting technique. J. Brazilian Soc. Mech. Sci. Eng. **41**(6), 267 (2019)
34. Cerri, E., Ghio, E.: Aging profiles of AlSi7Mg0. 6 and AlSi10Mg0. 3 alloys manufactured via laser-powder bed fusion: direct aging versus T6. Materials. **15**(17), 6126 (2022)
35. Saban, Ö., Korkmaz, M.E., Unal, O., Gok, M.S., Erdoğan, A.: Tribological, microstructural and surface characteristics of additively manufactured AlSi10Mg to sequential vibratory peening and heat treatment. Surf. Coat. Technol. **511**, 132307 (2025)
36. Subramaniyan, A.K., Reddy, A.S., Mathias, S., Shrivastava, A., Raghupatruni, P.: Influence of post-processing techniques on the microstructure, properties and surface integrity of AlSiMg alloy processed by laser powder bed fusion technique. Surf. Coat. Technol. **425**, 127679 (2021)

Figures

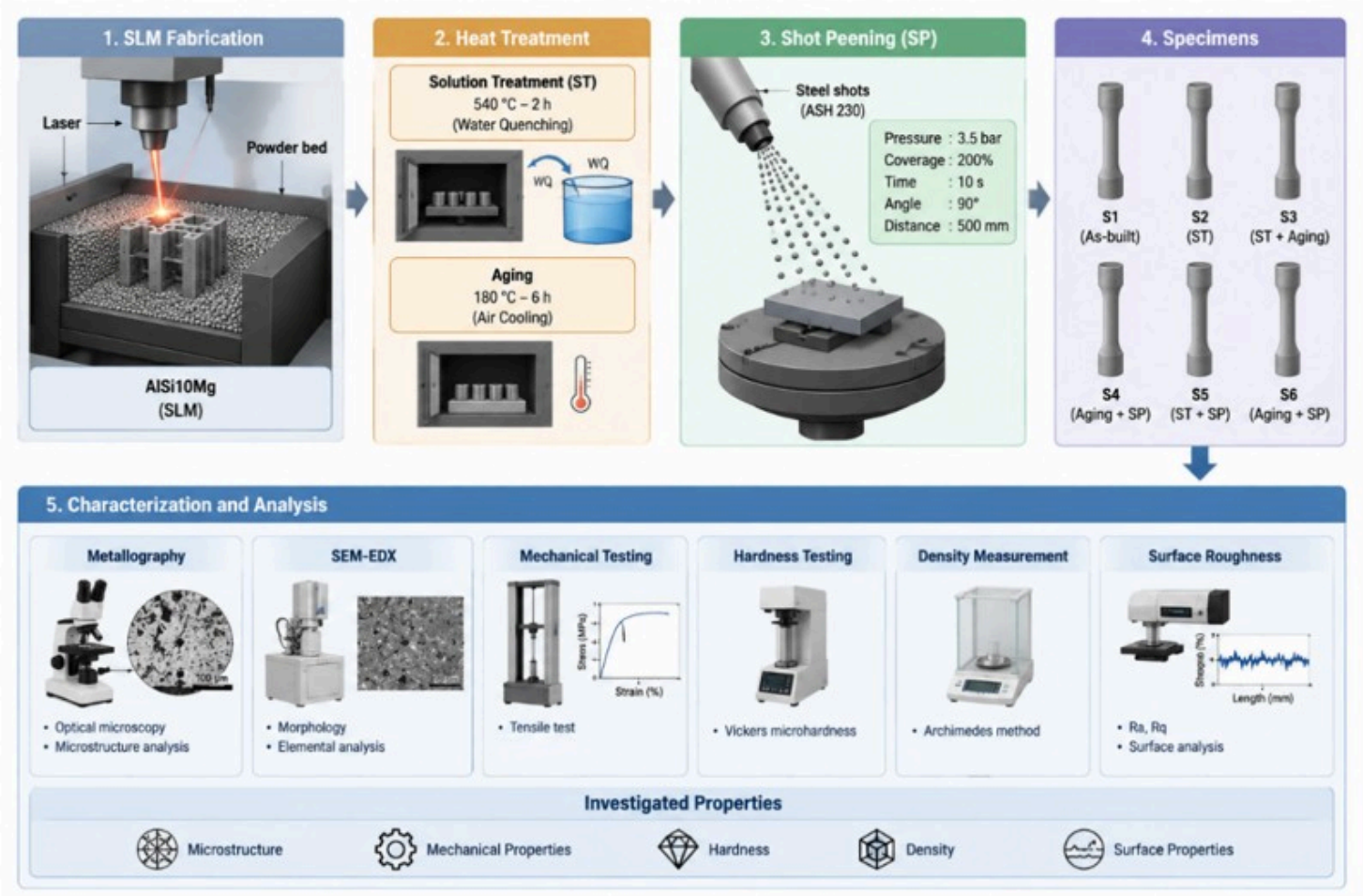


Figure 1

Schematic representation of the experimental process and characterization procedures for SLMed AlSi10Mg.

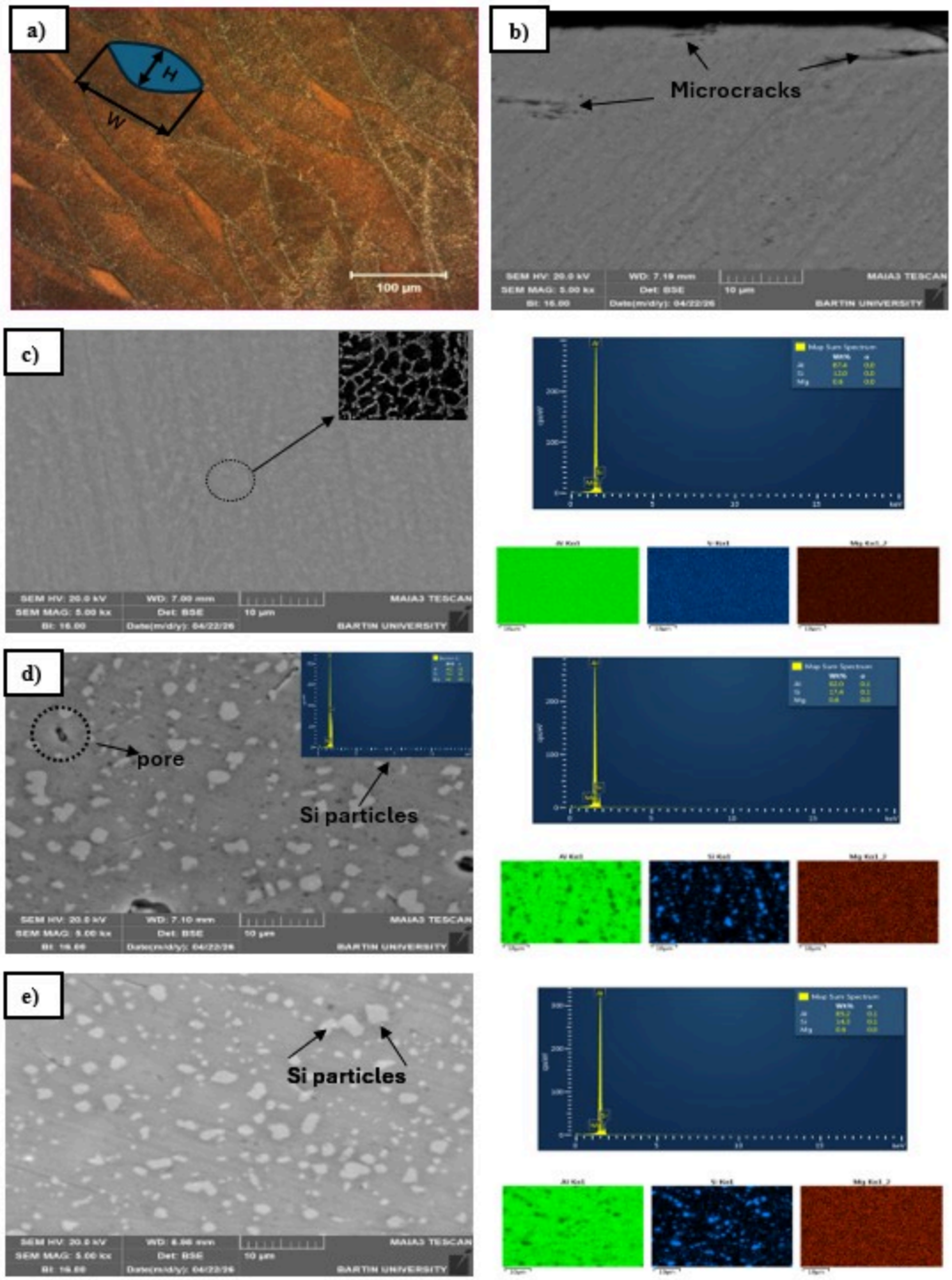


Figure 2

Metallographic images of SLM-processed AlSi10Mg: a) as-built optical microscope image, b) SEM image after shot peening, c) as-built SEM image with EDX analysis, d) SEM image with EDX analysis after ST, e) SEM image with EDX analysis after aging.

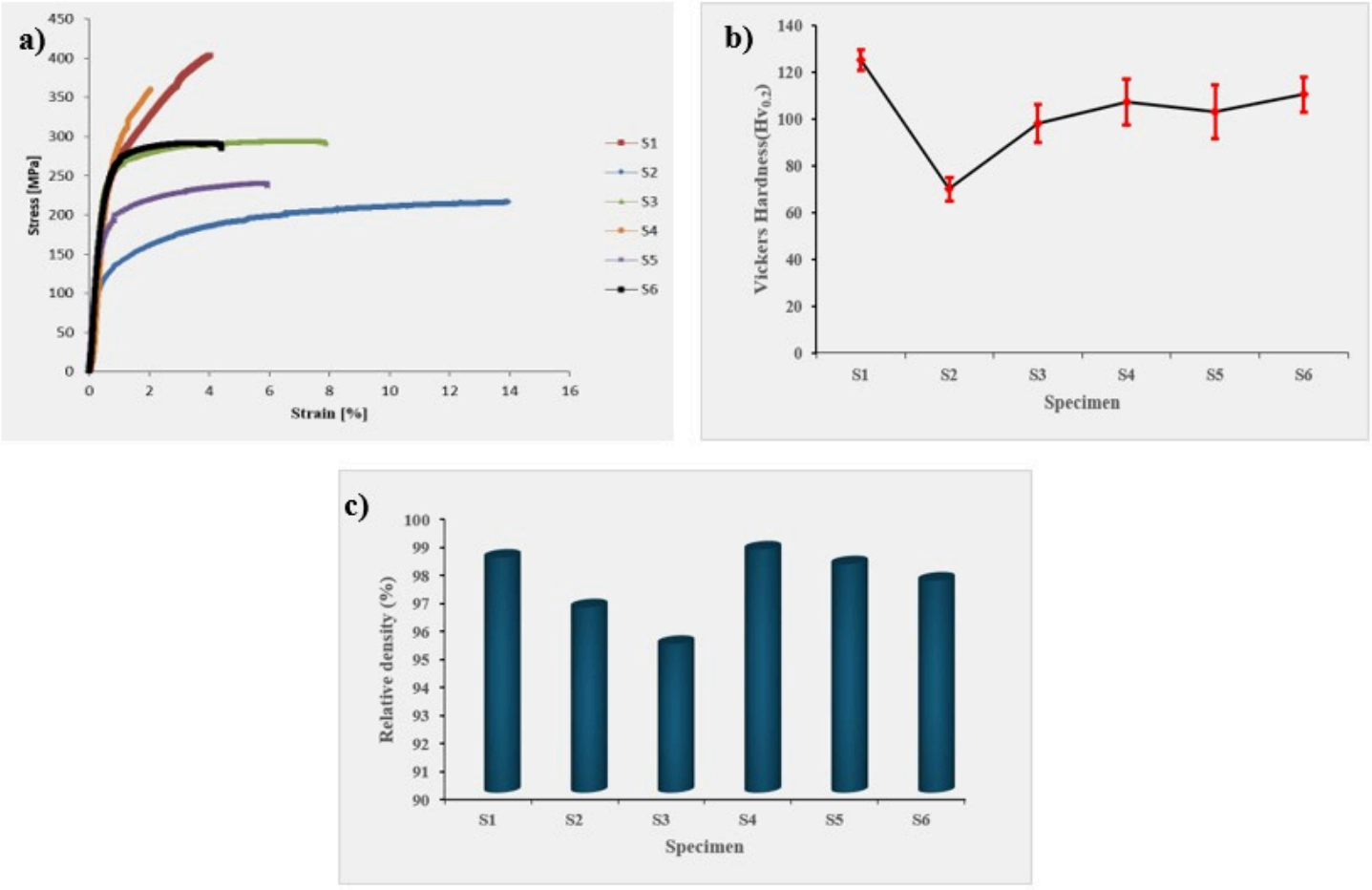


Figure 3

Comparison of mechanical properties, Vickers microhardness, and density of SLMed AlSi10Mg specimens under different post-processing conditions.

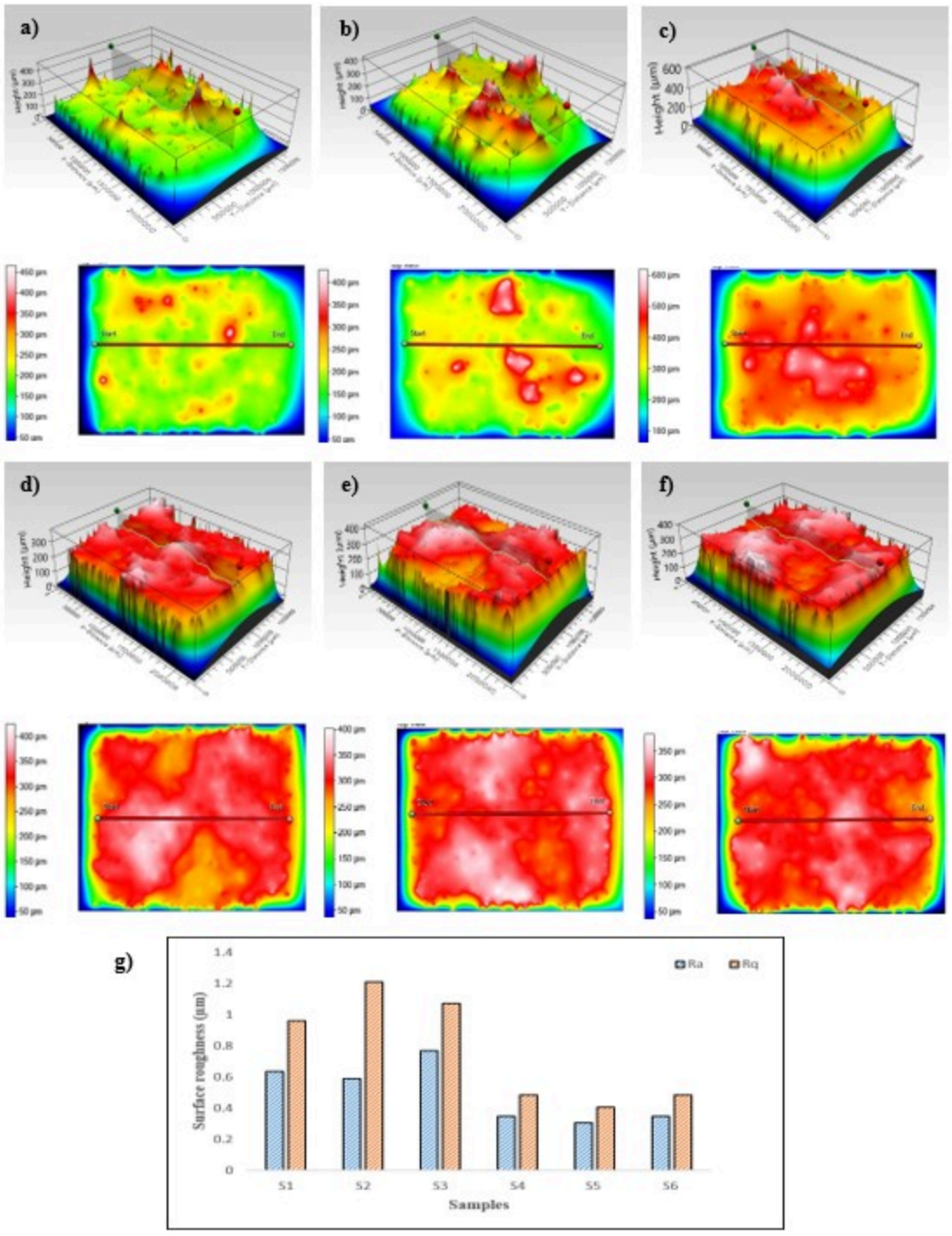


Figure 4

Surface topographies and roughness parameters (Ra and Rq) of SLMed AlSi10Mg specimens under different post-processing conditions.